Archaeometry

WILEY

ORIGINAL ARTICLE OPEN ACCESS

Investigating Technology and Raw Materials Source of the Archaic and Classical Architectural Terracottas From the *Athenaion* in Castro (Apulia, Italy)

M. M. N. Franceschini[1,2] | T. Ismaelli[1] | S. Vettori[1] | L. Chelazzi[3] | S. Ciattini[3] | F. Di Benedetto[1,4] | C. Grifa[5] | E. Cantisani[1]

[1]CNR-ISPC - Institute of Heritage Science, Sesto Fiorentino (Florence), Italy | [2]UNIROMA1, Department of Science of Antiquities, Sapienza University of Rome, Rome, Italy | [3]CRIST - Centre of Structural Crystallography, University of Florence, Sesto Fiorentino (Florence), Italy | [4]DFST, Department of Physics and Earth Science, University of Ferrara, Ferrara, Italy | [5]UNISANNIO, DST, Department of Science and Technology, University of Sannio, Benevento, Italy

Correspondence: E. Cantisani (emma.cantisani@cnr.it)

Received: 20 July 2025 | **Revised:** 27 September 2025 | **Accepted:** 11 November 2025

Keywords: Castro (Apulia) | petrography | production technology | raw materials source | terracotta | X-ray diffraction | X-ray fluorescence

ABSTRACT

Since 2000, archaeological excavations have brought to light the sanctuary of Athena in Castro (Apulia, Italy), including terracotta roofs dated between the 6th and 4th centuries BCE. Based on their morphological and stylistic features, it is suggested that the terracotta items were manufactured in the Greek colony of Taras (modern Taranto); conversely, several fragments cannot yet be confidently attributed to any specific production site. To shed light on the technology and the provenance of terracotta roof samples, 20 fragments were investigated using mineralogical and petrological techniques, revealing the presence of four compositional groups featured by different ratios of carbonate and volcanic inclusions. The mineral chemistry of the volcanic component opened interesting geoarchaeological and volcanological issues since it can be ascribed to one of the pyroclastic deposits from Ischia. Finally, these findings provided new insights into terracotta production in Taras, illuminating raw material sourcing, trade routes and technological skills.

1 | Introduction

The sanctuary of Athena in Castro (Lecce province, Apulia; Figure 1) was continuously frequented from the 8th century BCE until its destruction during the Second Punic War at the end of the 3rd century BCE (D'Andria 2009, 2020; D'Andria et al. 2023). Located in a position of strategic importance for southern Adriatic navigation, it was managed for centuries by the indigenous Messapian elites. However, it attracted not only local communities but also Greeks from Taras (a Spartan colony, modern Taranto) and the opposite Adriatic coast (Figure 1). Serving as an emporium—a sacred space that encouraged trade and cultural exchange—the sanctuary played a key role in connecting diverse populations. It is worth noting that from the 6th century BCE, craftsmen from Taras were entrusted with the construction of stone temples, shrines, altars and terracotta roofs. In fact, distinctive morphological features, structural solutions and decorative motifs of the terracotta roofs strongly suggest the involvement of artisans from Taras in their production (Ismaelli 2023).

This paper first aims to verify the proposed hypothesis and then addresses a crucial question about the production process of terracotta roofs. Two potential scenarios are considered for the construction of the roofs of the sanctuary of Athena. In the first scenario, artisans from Taras may have worked directly on-site in Castro, establishing nearby workshops to select, process, shape and fire the clay pieces before assembling the roof

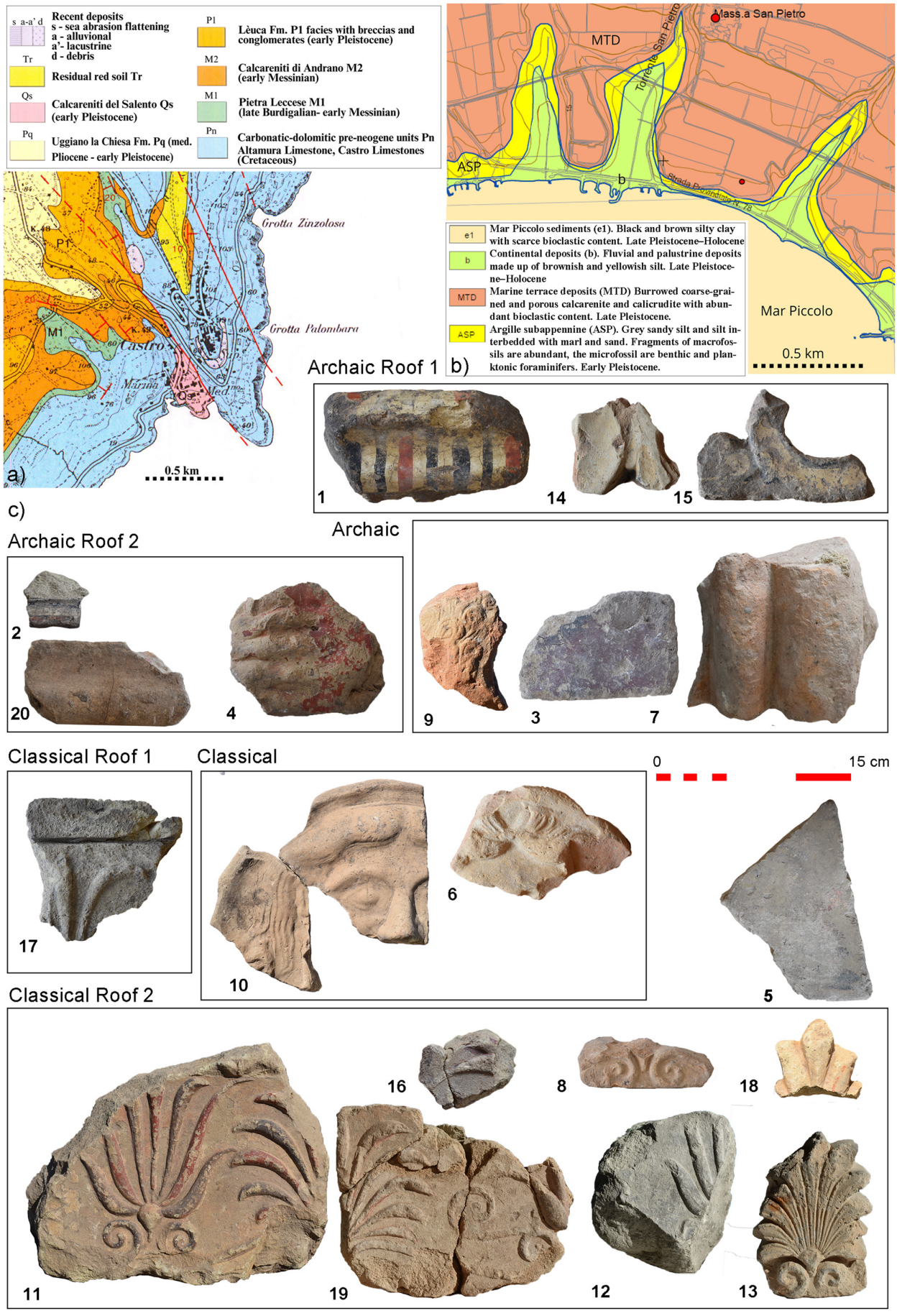

FIGURE 1 | Legend on next page.

FIGURE 1 | (a) Geological map of the area of Castro (modified after Bossio et al. 1997); (b) geological map of the Mar Piccolo area, north of Taranto (modified after Lisco et al. 2016); (c) the sampled terracotta roof elements from the Athenaion at Castro.

components. In the second scenario, the terracotta pieces were likely produced in Taras using local raw materials and then transported by sea—approximately 90 nautical miles (170 km)—to the sanctuary for their final assembly.

Thus, the identification of the source of raw materials through archaeometric analysis aims to determine whether the production occurred locally at Castro or in Taras, thereby providing a more precise understanding of the organization of labour and resources, as well as the transfer of raw materials or finished products for the construction of the sanctuary of Athena.

2 | Investigated Archaeological and Geological Materials

A total number of 20 fragments of architectural terracotta were collected, and their morphological, stylistic, and dimensional characteristics, along with fabric analysis, made it possible to assign the roofing elements to two distinct chronological phases:

2.1 | Archaic Period

Archaic Roof no. 1 is represented by fragments nos. **1, 14** and **15**, featuring a compact, refined ceramic body ranging from yellowish to orange-pink, with a white-yellowish slip that appears highly glossy in fragment no. 1. These pieces belong to a *sima* painted with Doric leaves and crowned by a chain of palmettes, dated to 530–500 BCE (see comparison in Rescigno 2023, 133–134).

Archaic Roof no. 2 includes fragments nos. **2** and **20**, characterized by a fine-grained, compact ceramic body in greenish-yellow and pinkish-orange hues and a yellowish slip. These fragments belong to the *geison* revetment (also called cassetta), decorated with an Ionic *cyma* on the lower moulding and swastika-meander on the soffit, dated to 530–500 BCE (Ismaelli 2023, 125–126, cat. nos. 98–100). Fragment no. **4**, corresponding to a leonine waterspout, may also belong to this roof.

The similarity in morphological details between Archaic Roofs no. 1 and no. 2 may suggest that they could belong to the same building, functioning as lateral side (no. 2) and raking cornice (no. 1).

To another Archaic roof are associated the following fragments: no. **3**, a tile made of brownish clay body, painted in a deep purplish-red hue; no. **7**, part of a ridge tile with torus mouldings; the antefix no. **9**, depicting a Gorgon's head with small snail-like curls with comparisons in Taras (Laviosa 1954, 233, no. 8, pl. 70, 1, late 6th century BCE; Berger 1982, 116–161, no. 161, before 480 BCE). Of uncertain chronology is the trapezoidal antefix no. **5**, composed of pinkish-beige clay, with a beige slip and trace of brown polychromy.

2.2 | Classical Period

Classical Roof no. 1 is represented by fragment no. **17**, which is part of a *sima* with a *cyma* as crowning moulding decorated with a palmette, composed of well-refined yellowish clay. A comparable specimen from Metapontum suggests a late 5th century BCE dating (Mertens-Horn 1988, 155–156, 205, cat. 74, pl. 80ab).

Other antefixes from the Classical period include no. **10**, a semicircular item with a Gorgon's head and lateral snakes, made from a worn mould also attested in Taras (Laviosa 1954, 235, no. 17, pl. 71, 4, second half of the 5th century BCE) and no. **6**, possibly representing a Gorgo's head with wavy hair pinned above the front (similar to Laviosa 1954, 236, no. 21, pl. 72, 3, late 4th–3rd century BCE; Dell'Aglio and Zingariello 2015, 33, end of the 5th century BCE).

To a later period is dated **Classical Roof no. 2**, represented by fragments nos. **11, 12, 16** and **19**, made of purified clay, varying in colour from yellowish-green to light brown. These fragments belong to a lateral and raking *sima* decorated in relief with egg-and-dart motifs, bead-and-reel and an *anthemion* of upright, open palmettes and lotus flowers, featuring red and brown polychromy (Magrini et al. 2023). This roof, based on comparisons with materials from the Tarentine colony of Herakleia (Policoro), can be dated to the late 5th—first half of the 4th century BCE (Ismaelli 2023, 126, cat. no. 102).

Additionally, palmettes nos. **8** and **13**, made of a very hard pinkish-beige clay, and the lotus flower no. **18**, featuring yellowish clay and traces of orange-brown colour, might have decorated the upper part of the *sima* of the Classical Roof 2 (see comparison in Cristofani 1967, 315–316, pl. 103).

In conclusion, between 530 BCE and the first half of the 4th century BCE, numerous roofs were constructed in the sanctuary of Athena for various buildings of different dimensions. This evidence indicates ongoing relationships between Greek artisans and Messapian ruling groups, with the origin, selection and treatment of raw materials providing key insights into these interactions.

The investigation into the provenance of raw materials led to the sampling of clay from deposits in both Castro and Taranto. In Castro, a site characterized by a clay outcrop within calcarenite formations was identified (Bossio et al. 1997), located to the east of the modern town. Sample C1 was gathered from the Parco delle Querce area, where clay has been extracted till recent times for local artisanal activities. A second sample collection was conducted in the Taranto area, where a significant clay deposit is located north of Mar Piccolo (sample C2). This zone had been previously investigated (De Marco et al. 1981; Valenzano et al. 2018). Instead, it is no longer possible to collect clay samples directly from the area of the ancient city, due to the modern extensive urban development, which has

covered areas where clay outcrops were still visible in the post-World War II period.

To further verify the provenance of the raw materials, two artifacts produced in Taranto were also analysed. Sample T1 is a fragment of a tile of the Greek period found in the area of Torre d'Ayala, made from greenish-yellow clay, discovered in Taranto in the late 1950s to early 1960s during modern construction work. Sample T2 is a modern terracotta object made from clay collected in the southern area of the city, near the Mar Grande, specifically in the Torre d'Ayala area during the late 1950s, when clay deposits were still accessible.

3 | Analytical Techniques

The petrographic characteristics of the terracotta samples were determined by observing thin sections with a Polarized Light Microscope (PLM), Zeiss Axioscope A.1., following the methodologies established by Whitbread 1989, Quinn 2009 and Quinn 2013. The microscope is equipped with a camera that has a 5-megapixel resolution and utilizes AxioVision image analysis software.

The quantitative mineralogical composition was determined by X-ray powder diffraction (XRPD). X'Pert Pro PANalytical diffractometer, equipped with an X'Celerator detector, with Cu X-ray tube ($\lambda = 1.5406$ Å) and a Ni-filtered Cu Kα radiation source, was used. An internal standard (LiF 15 wt%) was employed to enable the determination of the amount of the glass or amorphous phases besides the crystalline ones (Ohbuchi et al. 2021). The use of lithium fluoride was necessitated by the requirement to utilize the same powder for chemical analysis, due to the small quantity of sample material, and both Li and F are elements too light to interfere during XRF analysis. The diffraction patterns were recorded under the following conditions: current of 30 mA, voltage of 40 kV, an explored 2θ range of 3°–120°, step size of 0.0167° and a total time per pattern of 3 h and 7 min.

Major, minor, and trace element compositions were determined using X-ray fluorescence (XRF). Thirteen samples were analysed using Wavelength Dispersive XRF (WDXRF) on a Rigaku ZSX Primus II with an Rh source after being fused with lithium borate at 1100°C. Calibration was performed using 26 geological reference materials from the Centre de Recherches Pétrographiques et Géochimiques of the French CNRS, which accounted for matrix effects and elemental overlaps. Although this method is accurate, it is destructive and requires several grams of sample material. Consequently, only 13 out of the 20 samples were analysed (nos. 1, 2, 4, 5, 6, 7, 14, 15, 16, 17, 18, 19 and 20). Due to the limited material available, the remaining seven samples were analysed using non-destructive Energy Dispersive XRF (EDXRF, Shimadzu EDX-7000, Rh source) on pressed powder placed in PTFE cups sealed with Mylar films. The same reference materials were used for calibration and the results from WDXRF were employed to validate the EDXRF measurements. Results include 10 major/minor oxides (SiO_2, Al_2O_3, Fe_2O_3, MnO, MgO, CaO, Na_2O, K_2O, TiO_2, P_2O_5 in wt%) and 8 trace elements (V, Cr, Ni, Cu, Zn, Sr., Zr, Ba in ppm), with analytical uncertainties. Cr was excluded from EDXRF-only samples due to poor calibration. Sample 13 was not analysed due to insufficient quantity.

The micro-textural and microchemical analyses of the terracotta component were performed using a SEM-EDS (ZEISS EVO MA 15) with W filament equipped with an energy dispersion EDS/SDD analysis system, Oxford Ultimax 40 (40 mm^2 with a resolution of 127 eV @5.9 keV) with Aztec 5.0 SP1 software. Polished thin sections were analysed under the following conditions: acceleration potential of 15 kV, 500 pA beam current, working distance between 9 and 8.5 mm; 20 s live time as acquisition rate to archive at least 600,000 cts, quantitative Co standard, process time 4 for point analyses; 500 μs pixel dwell time to acquire maps with a resolution of 1024 × 768 pixels. The program used for the microanalysis was Aztec 5.0 SP1 software using the XPP matrix correction scheme developed by Pouchou and Pichoir (1991).

Moreover, the two clay samples (C1 and C2) and the two artefacts from Taranto (T1 and T2) were also analysed by semi-quantitative XRPD and XRF; in addition, T1 and T2 were also analysed using PLM.

4 | Results

4.1 | Polarized Light Microscope (PLM)

Four petrographic groups were identified based on the clay matrix characteristics and the abundance, composition, and morphology of the aplastic inclusions. Table 1 summarizes the results of the analyses.

4.1.1 | Group A

Group A is composed of samples belonging to Classical Roof no. 2, represented by fragments nos. 11, 12, 16, 18 and 19. These samples consist of a grey-coloured clay matrix with low birefringence and no optical activity. Aplastic inclusions represent 20%–30% of the composition (Figure 2a). The coarse-grained inclusions are primarily volcanic materials, mainly occurring as glass fragments, pumice, and shards. Rare lava fragments exhibit a microcrystalline texture characterized by plagioclase, or a hyaline texture containing feldspar microcrystals. Additionally, the samples contain dark grains with sharp boundaries, known as argillaceous rock fragments (ARF). Overall, the porosity of the samples is generally low.

4.1.2 | Group B

Group B is composed mainly of samples belonging to Archaic Roofs 1 (sample 1) and 2 (samples 2, 4 and 20) and samples nos. 3 and 5 from other Archaic roofs. These samples consist of a brown-grey clay matrix with moderate optical activity. The percentage of aplastic inclusions ranges from 20% to 30% (Figure 2b). Feldspar crystals, which reach a maximum size of 0.725 mm, and clinopyroxene are rare, as well as lava fragments, which are mostly rounded and exhibit either a microcrystalline texture of plagioclase or a hyaline texture with microcrystals of

TABLE 1 | Petrographic description of the four groups of terracotta samples.

Group ID	Matrix		Inclusions content%	Porosity		Aplastic inclusions												Max sizes (mm)	Min sizes (mm)	Mean size (mm)	Shape
						Coarse							Fine								
	Colour	Optical activity		Pore shape	Repr.	vgf	feld	cpx	mrf	crf	fs	qz	vgf	cpx	feld	phy	fs	qz				
Group A	Grey	Absent	20%–30%	Low	Sub-rounded—sub-angualar elonged iso-oriented	a	d	b	a	tr				d		c				0.6 0.8	0.04 0.055	0.11 0.19	Mostly angular
Group B	Brown-grey	— moderate	20%–30%	Low	Mostly amorphous (rarely sub-rounded)	a	d	a	a	tr			tr	c	c	d			tr	0.4 0.8	0.0035 0.05	0.095 0.145	Mostly angular
GROUP C	Brown	Medium	30%–40%	Low	Sub-rounded elonged	a	c	a			a			c	c	d				0.4 0.65	0.035 0.05	0.095 0.145	Mostly angular
Group D	Brown-orange	Medium-high	30%–40%	Low	Sub-rounded	a	a	tr			a	a	b	b	a	d	b	b	c	0.3 0.5	0.04 0.055	0.0950.145	Mostly angular

Abbreviations: cpx, clinopyroxene; crf, carbonatic rock fragments; feld, feldspars; fs, fossilis; mrf, magmatic rock fragments; phy, phyllosilicates; qz, quartz; vgf, volcanic glass fragments.
[d]predominant.
[c]abundant.
[b]frequent.
[a]present; tr trace. Repr. = reprecipitation of calcite in the pores.

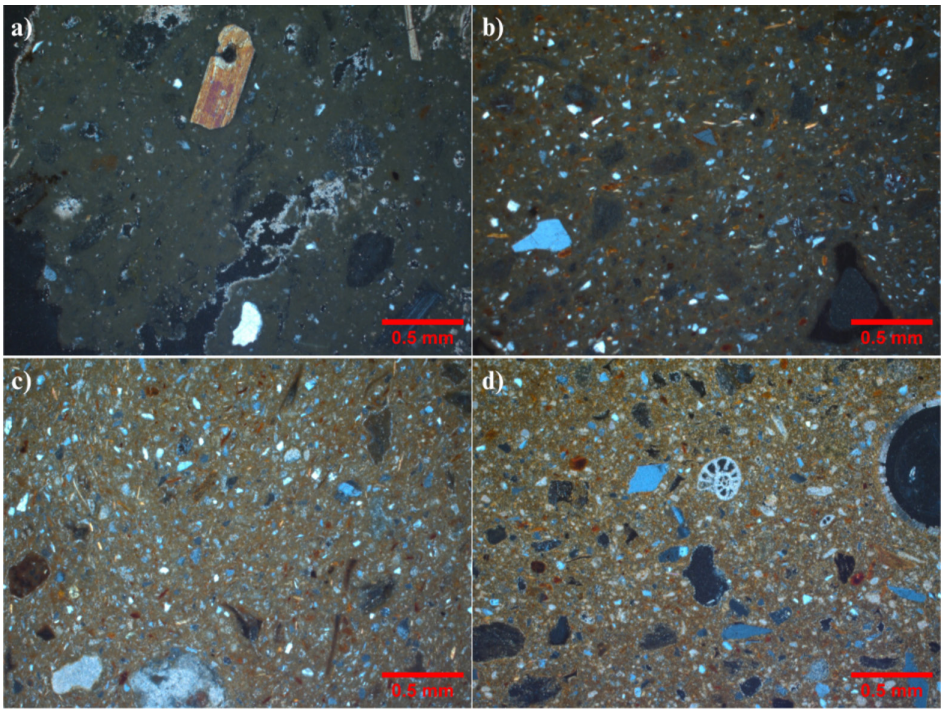

FIGURE 2 | Microphotographs of thin sections, representative of the four petrographic groups; (a) sample 12; (b) sample 4; (c) sample 14; (d) sample 7 (cross-polarized light).

feldspar. Pumices and small feldspars are common. The porosity of the samples is low. It is important to note that petrographic Group B is divided into two subgroups (B1 and B2). Subgroup B1 includes samples 1, 2 and 3, characterized by a greyish matrix with low optical activity, while subgroup B2 consists of samples 4, 5 and 20, which feature a brownish matrix with medium to low optical activity.

4.1.3 | Group C

Group C contains samples nos. 14 and 15 from Archaic roof 1, sample no. 13 from Classical roof 2 and sample no. 17 from Classical roof 1. These samples have a brown clay matrix. Their optical activity ranges from medium to low. The content of aplastic inclusions is between 30% and 40% (Figure 2c). These aplastic inclusions mainly consist of crystals and volcanic glass, with small amounts of feldspar, elongated phyllosilicates and rare acicular clinopyroxene crystals that are likely newly formed. Additionally, there are some lithic carbonate fragments and few larger feldspar crystals. The overall porosity is low. Sample 17 contains carbonates and aplastic inclusions that closely resemble those found in Group C; however, the optical properties of its clay matrix are more similar to those of Group B samples. Therefore, sample 17 can be considered an outlier for both groups.

4.1.4 | Group D

Group D contains samples nos. 7 and 9 dated to the Archaic period, sample no. 6 is of the Classical period, while sample no. 8 belongs to Classical roof 2. The samples have a clay matrix that ranges in colour from brown to orange, with sample 7 appearing almost yellow. The optical activity is medium to high. The content of aplastic inclusions is approximately 30%–40% (Figure 2d). Common components include small feldspars, quartz, tiny acicular phyllosilicates and clinopyroxene crystals. Carbonate fragments, such as shell fragments and microfossils, are also frequently observed. Notably, volcanic glass fragments are absent in sample 9. Only sample 7 contains small lava fragments featuring a fluidal microcrystalline plagioclase texture or a hyaline texture with feldspar microcrystals. The maximum size of the aplastic inclusions in these samples is about 0.3–0.5 mm, except in sample 7, where the inclusions can reach 0.65–0.7 mm. Overall, the porosity is low.

The two artifacts from Taranto are described as follows: T1 has a grey clay matrix with low optical activity. It contains volcanic glass, feldspar crystals measuring up to 1.5 mm and rare clinopyroxene crystals reaching up to 600 μm. In contrast, T2 features an orange-coloured matrix with medium to high optical activity. This artifact includes small feldspar and phyllosilicate crystals, benthic foraminifera fossils, carbonate lithics measuring up to 600 μm and rare volcanic glass and volcanic lithics.

4.2 | QXRPD

The quantitative mineralogical data are listed in Table 2, some examples of Rietveld refinement are reported in Figure S1.

The crystalline phases, outlined by the bulk mineralogical paragenesis, consist of minerals found in both aplastic inclusions and the clay matrix—components that are not visible under polarizing optical microscopy. All samples contain varying amounts of diopside, quartz, albite, analcime, gehlenite, anorthite, calcite, microcline, muscovite, wollastonite and hematite. In the analysed samples, the amorphous phases either originate

TABLE 2 | Quantitative results of the Rietveld analysis of the bulk terracotta samples. Percentages of amorphous and crystalline phases are listed, mineralogical phases are normalised to 100%.

	Samples	Amorp.	Cryst.	Di	Qz	Ab	Anl	Gh	An	Cal	Mc	Ms	Wo	Hem
Group A	**11**	37.0	63.0	38	6.3	0.4	14.1	2.5	21.0	1.7	8.9	4.5	2.5	0.1
	12	31.9	68.1	38.3	4.0	0.4	13.2	1.2	25.7	0	11.0	3.4	2.6	0
	16	54.0	46.0	34.6	11.8	1.9	12.6	5.7	14.8	3.6	6.1	6.8	2.1	0.1
	18	51.1	48.9	37.6	7.3	6.5	14.6	2.1	19.9	0	6.2	4.2	1.6	0.1
	19	48.5	51.5	30.3	11.6	2.4	10.3	8.3	20.8	3.1	4.0	6.8	2.2	0.1
Group B	**1**	39.1	60.9	22.2	16.1	8.4	10.4	8.5	20.9	1.9	4.0	5.9	1.5	0.2
	2	51.1	48.9	26.8	13.7	0.9	11.5	8.1	22.1	6.0	3.2	5.8	1.7	0.2
	3	17.2	82.8	29.9	17.6	0.6	10.7	10.2	15.4	0.4	5.4	5.8	3.7	0.2
	4	54.4	45.6	18.5	22.0	2.3	7.1	10.0	20.9	2.2	7.2	6.5	2.9	0.4
	5	50.1	49.9	19.7	20.3	1.5	5.1	9.8	23.4	3.8	8.7	5.3	2.0	0.4
	20	59.2	40.8	18.2	20.1	4.3	9.6	9.6	15.3	7.5	5.9	7.3	1.7	0.4
Outlier	**17**	62.7	37.3	29.0	16.2	7.0	7.2	9.0	14.3	2.7	5.9	5.2	3.2	0.3
Group C	**10**	51.5	48.5	14.0	30.4	1.2	1.1	12.5	17.2	9.8	2.0	10.0	1.0	0.8
	14	56.1	43.9	14.6	32.8	2.4	0	5.2	18.0	10.8	5.9	9.0	0.8	0.7
	15	52.2	47.8	16.3	25.4	1.9	5.7	11.3	14.4	7.6	5.9	8.4	2.6	0.6
Group D	**6**	57.8	42.2	2.7	33.7	6.7	0.3	2.6	10.0	20.2	10.7	12.1	0.3	0.7
	7	67.6	32.4	2.7	31.8	4.8	0.5	0.6	7.3	26.2	6.6	18.6	0.3	0.7
	8	57.9	42.1	16.9	31.3	5.6	0.6	3.2	9.2	16.1	4.8	10.8	0.4	1.1
	9	33.6	66.4	7.6	33.2	2.4	0	6.1	15.4	20.7	4.4	9.7	0.1	0.5

Abbreviations according to Whitney and Evans 2010: Ab, albite; Anl, analcime; An, anorthite; Cal, calcite; Di, diopside; Hem, hematite; Gh, gehlenite; Mc, microcline; Ms, muscovite; Qz, quartz; Wo, wollastonite.

from inclusions of volcanic glass or result from the structural breakdown of phyllosilicates during firing temperatures exceeding 450°C (Quinn 2013). According to Rietveld analysis, the amorphous content (mean value) is highest in Group D at 54.2%, followed by Group C at 53.4%, Group B at 48.5% and Group A at 44.4%. Worth noting, QXRPD analyses corroborate the petrographic observations, consistently grouping the samples according to some key mineralogical parameters.

Group A predominantly consists of abundant diopside (30.3%–38.3%), analcime (10.3%–14.6%), and anorthite (14.8%–25.7%). Calcite is present in amounts below 3.6% and is absent in samples 12 and 18. Muscovite ranges between 3.4% and 6.8%, while quartz is relatively low, ranging from 4% to 11.8%.

Group B, which includes the outlier sample 17, contains diopside (18.2%–29.9%), analcime (5.1%–11.5%) and anorthite (14.3%–23.4%). The calcite content is generally below 3.8%, except in samples 2 and 20, where it is 6.0% and 7.5% due to recrystallization. Quartz varies between 13.7% and 22%, while muscovite ranges from 5.3% to 7.3%. Additionally, Group B shows two subgroups based on mineralogical differences:

Subgroup B1 (samples 1, 2, 3 and 17) has higher diopside (22.2%–29.9%) than quartz (13.7%–17.6%) and analcime between 7.2% and 11.5%. Subgroup B2 (samples 4, 5 and 20) has more quartz (20.1%–22.0%) than diopside (18.2%–19.7%) and analcime between 5.1% and 9.6%.

Group C has a higher content of calcite (7.6%–10.8%), quartz (25.4%–32.8%), and muscovite (8.4%–10.0%), with a lower diopside content (14%–16.3%).

Group D is characterized by the highest amounts of calcite and muscovite, along with the lowest content of volcanic minerals. Samples 6 and 7 contain minimal diopside, at 2.7%, and high levels of calcite, which are 20.2% and 26.2%, respectively. Samples 8 and 9 have calcite contents of 16.1% and 20.7%, respectively, with varying levels of diopside: 16.9% in sample 8 and 7.6% in sample 9. Muscovite is abundant in this group, ranging from 9.7% to 18.6%, while quartz levels fluctuate between 31.3% and 33.7%. Analcime is absent, and anorthite content ranges from 7.3% to 15.4%. This variability suggests the possibility of internal subgrouping within Group D. Additionally, samples 6 and 7 contain very little clinopyroxene (under 3%), whereas samples 8 and 9 exhibit higher diopside levels, making them mineralogically similar to Group C.

4.3 | XRF

The terracotta samples exhibit only a limited range of compositional variability, both in their major, minor and trace

components. This limited variability does not allow the petrographic and mineralogical grouping to be distinguished. This information is detailed in Table 3 and illustrated in Figure S2a,b. However, chemical composition permits the comparison of terracottas with the clay materials (C1 and C2) and Tarentine artefacts.

Sample C1, coming from the Castro area, is characterized by a higher concentration of CaO (44.27 wt%) and lower levels of SiO_2 (17.25 wt%) and Al_2O_3 (5.54 wt%) compared to C2, which comes from the Taranto area (CaO 17.06 wt%; SiO_2 46.48 wt%; Al_2O_3 13.58 wt%). In addition, T1 and T2 exhibit CaO contents of 16.53 wt% and 19.96 wt%, respectively, with SiO_2 levels of 50.77 wt% and 46.58 wt% and Al_2O_3 levels of 15.21 wt% and 11.07 wt%.

In terms of trace elements, C1 contains lower concentrations of Sr., Zr and Ba (270, 58 and 66 ppm, respectively), but a higher concentration of Ni (296 ppm) compared to the terracotta samples and C2, T1 and T2.

4.4 | SEM-EDS

Samples 2, 4, 7, 12, 14, 16, 19 and T1 were analysed using SEM-EDS. The chemistry of volcanic glasses, feldspar and pyroxene is detailed in Table S1.

Figure 3a illustrates the classification of feldspars based on the ternary An-Ab-Or diagram (Deer et al. 2013). Sanidine is consistently present in the terracotta samples. Sample 16 contains anorthite and bytownite, while sample 19 includes bytownite along with several Na-rich plagioclases (oligoclase and albite) and K-feldspars (sanidine and anorthoclase).

Clinopyroxenes were classified according to the Morimoto diagram (Morimoto et al. 1988) and exhibit a composition ranging from diopside to hedenbergite (Figure 3b). All samples feature chemically zoned clinopyroxenes. In samples 2, 7 and 12, the clinopyroxenes display reverse zoning (Figure 3c,d), with rims that have a diopside composition and are richer in Mg compared to their cores (which are composed of wollastonite-hedenbergite, rich in Ca and Fe). In samples 16 and 19, the clinopyroxenes have cores made of diopside that evolve into hedenbergite-wollastonite, capped by an outer rim of diopside.

The TAS diagram (Le Bas et al. 1986) was utilized to classify the juvenile samples (Figure 3e). Samples 4 and 14 predominantly contain juveniles with phonolitic glass compositions, while samples 7 e12 primarily consist of trachyte. Additionally, the glasses in samples 16 and 19 are more varied, with a majority being trachytic. In these samples, we rarely observe glasses with tephriphonolitic or trachyandesitic compositions. By examining the chemical composition of the glasses and analysing the ratio of alkalis (Na/K), we found that most of the volcanic glasses examined show a sodic affinity. The volcanic glass contained in the sample T1 shows a mainly trachytic composition, rather similar to the compositions already observed in the volcanic glass present in the Castro terracotta samples.

5 | Discussion

5.1 | Provenance of Raw Materials

The ternary ACS (Al_2O_3–CaO–SiO_2) diagram (Levin et al. 1964), which is based on four petrographic groups, classifies all analysed samples as calcium-rich terracottas made from a carbonate-bearing clay sediment (Figure 4). Additionally, the clay samples are represented in the diagram: the chemical composition of sample C2 is similar to that of the terracotta samples (refer to Figure 4 and Table 3), while sample C1 displays a significantly different chemical composition. Notably, the two artifacts from Taranto (T1 and T2) fall within the same group.

In discussing the origin of the raw materials used in terracotta production, it is important to highlight that most of the non-plastic inclusions in all the samples consist of volcanic rock fragments. Volcanic inclusions serve as significant indicators of provenance because they reflect a limited and well-defined geological context. Clear examples can be found in pottery production from areas such as the Bay of Naples, Sicily and other volcanic regions (Germinario et al. 2019; Rodríguez et al. 2015; Pérez-Monserrat et al. 2023; Izzo et al. 2021; Barone et al. 2010; Bajnok et al. 2022).

However, it is worth noting that volcanic sediments and tephra are relatively rare in Apulia and are primarily concentrated in the northern part of the region. This is particularly evident in the Tavoliere delle Puglie and Gargano, where tephra from the Somma-Vesuvius (Campania) and the Vulture volcano (Basilicata) can be found (Cioni et al. 2000; Donato et al. 2022; De Santis and Caldara 2015; Bosellini et al. 1999; Sansò et al. 2015). On the other hand, the only evidence of a tephra, so far reported, in the southern part of Apulia, is the deposit of the Y-7 eruption from the Ischia volcano (~60 ± 2.2 ky BP) (D'Antonio et al. 2021) (Figure S3).

The first match between the tephra from the Y-7 eruption and the volcanic clasts found in the terracotta from Castro can be confirmed through the mineral and juvenile composition analysed using SEM EDS. The chemical composition of ferrian diopside exhibits reverse zoning, which is a typical characteristic of the pyroxenes associated with the Y-7 eruption (D'Antonio et al. 2021; Brown R. et al. 2014). Additionally, the feldspar and juvenile compositions range from trachyte to phonolite, with a tendency towards more sodic compositions. All of these are consistent with those found in volcanic products from Ischia (Melluso et al. 2014; Vineberg et al. 2023).

Thus, there is a geochemical compatibility between the volcanic clasts found in the terracotta from Castro and the tephra from the Y-7 eruption. Additionally, using a calculation tool from volcanological research, a more detailed assessment of the production area can be proposed.

According to the LaMEVE database (Brown S. et al. 2014), the Y-7 eruption produced an eruptive column that reached more than 25 km in height, resulting in the injection of particles into the stratosphere. The Volcanic Explosivity Index (VEI) for the Y-7 eruption is estimated between 6 and 7. During such high-energy

TABLE 3 | Chemical composition of the investigated samples, from WDX and EDX (*) XRF analyses. The relative uncertainty, extrapolated from the calibration curves, is also listed.

	SiO_2	Al_2O_3	Fe_2O_3	MnO	MgO	CaO	Na_2O	K_2O	TiO_2	P_2O_5	V	Cr	Ni	Cu	Zn	Sr	Zr	Ba
	wt%	wt%	wt%	wt%	wt%	wt%	wt%	wt%	wt%	wt%	ppm	ppm	ppm	ppm	ppm	ppm	ppm	ppm
1	48.66	12.49	4.88	0.11	2.96	12.74	1.98	1.30	0.57	0.47	83	123	114	43	89	434	214	307
2	47.01	11.77	4.47	0.09	2.86	14.92	1.83	1.11	0.54	0.15	101	122	86	35	75	415	190	312
3*	46.86	12.35	3.46	0.10	2.61	14.61	2.34	1.00	0.45	0.36	117	nd	89	33	103	415	172	372
4	50.21	13.21	4.97	0.11	2.56	10.41	1.59	2.10	0.61	0.59	92	129	92	40	89	415	204	367
5	48.24	12.58	4.91	0.10	2.93	13.02	1.38	1.90	0.59	0.43	89	128	107	43	86	467	188	337
6	44.26	9.40	3.73	0.07	1.92	14.47	0.57	1.91	0.46	0.32	89	76	59	45	64	304	142	218
7	43.43	10.92	4.19	0.09	2.27	13.67	0.93	2.83	0.50	0.18	93	94	83	36	69	399	178	310
8*	48.23	14.07	3.51	0.10	2.36	14.90	2.00	3.00	0.46	0.26	118	nd	96	51	94	363	157	353
9*	46.01	11.94	3.24	0.08	2.15	11.94	1.88	2.42	0.41	0.26	104	nd	94	25	78	249	121	306
10*	49.00	12.58	3.43	0.10	2.57	15.02	1.21	2.23	0.45	0.23	114	nd	98	31	109	336	139	314
11*	46.33	14.43	3.62	0.11	2.69	14.04	1.21	0.95	0.51	0.16	127	nd	93	41	98	481	197	291
12*	45.65	14.00	3.69	0.12	2.52	12.50	1.21	0.90	0.53	0.13	128	nd	97	26	100	474	198	208
14	49.19	11.56	4.73	0.09	2.67	11.43	0.85	2.57	0.56	0.55	73	115	101	44	83	335	173	300
15	47.73	11.99	4.71	0.09	2.52	13.60	1.38	1.96	0.56	0.22	91	122	90	39	74	406	183	323
16	46.65	13.15	5.11	0.10	3.05	14.65	1.81	1.40	0.59	0.30	122	142	100	38	79	522	193	337
17	49.73	12.47	4.89	0.09	2.87	12.98	1.44	1.70	0.57	0.34	92	138	98	44	79	390	176	346
18	48.63	14.23	5.54	0.10	3.08	11.96	2.34	1.40	0.63	0.19	109	148	106	43	76	509	211	311
19	44.35	12.45	5.05	0.09	2.54	15.31	1.86	1.30	0.60	0.14	94	133	99	34	84	495	189	278
20	48.13	12.36	4.63	0.10	0.67	13.14	0.22	1.78	0.56	0.33	85	117	86	38	76	398	199	324
C1	17.25	5.54	2.75	0.05	2.05	44.27	0.29	0.85	0.22	0.09	104	96	296	44	63	270	58	66
C2	46.48	13.58	5.89	0.08	3.92	17.06	0.41	2.36	0.61	0.11	122	209	268	28	93	520	132	281
T1	50.77	15.21	7.01	0.10	2.74	16.53	0.86	1.75	0.69	0.15	120	187	177	19	74	543	184	538
T2	46.58	11.07	4.31	0.08	3.24	19.96	0.69	2.09	0.50	0.10	89	137	163	23	75	501	166	260
% error	*4 (5)**	*4 (10)**	*3 (10)**	*5 (5)**	*5 (25)**	*5 (5)**	*5 (22)**	*5 (5)**	*4 (10)**	*8 (10)**	*4 (10)**	*6*	*8 (10)**	*9 (15)**	*7 (10)**	*5 (10)**	*6 (10)**	*6 (10)**

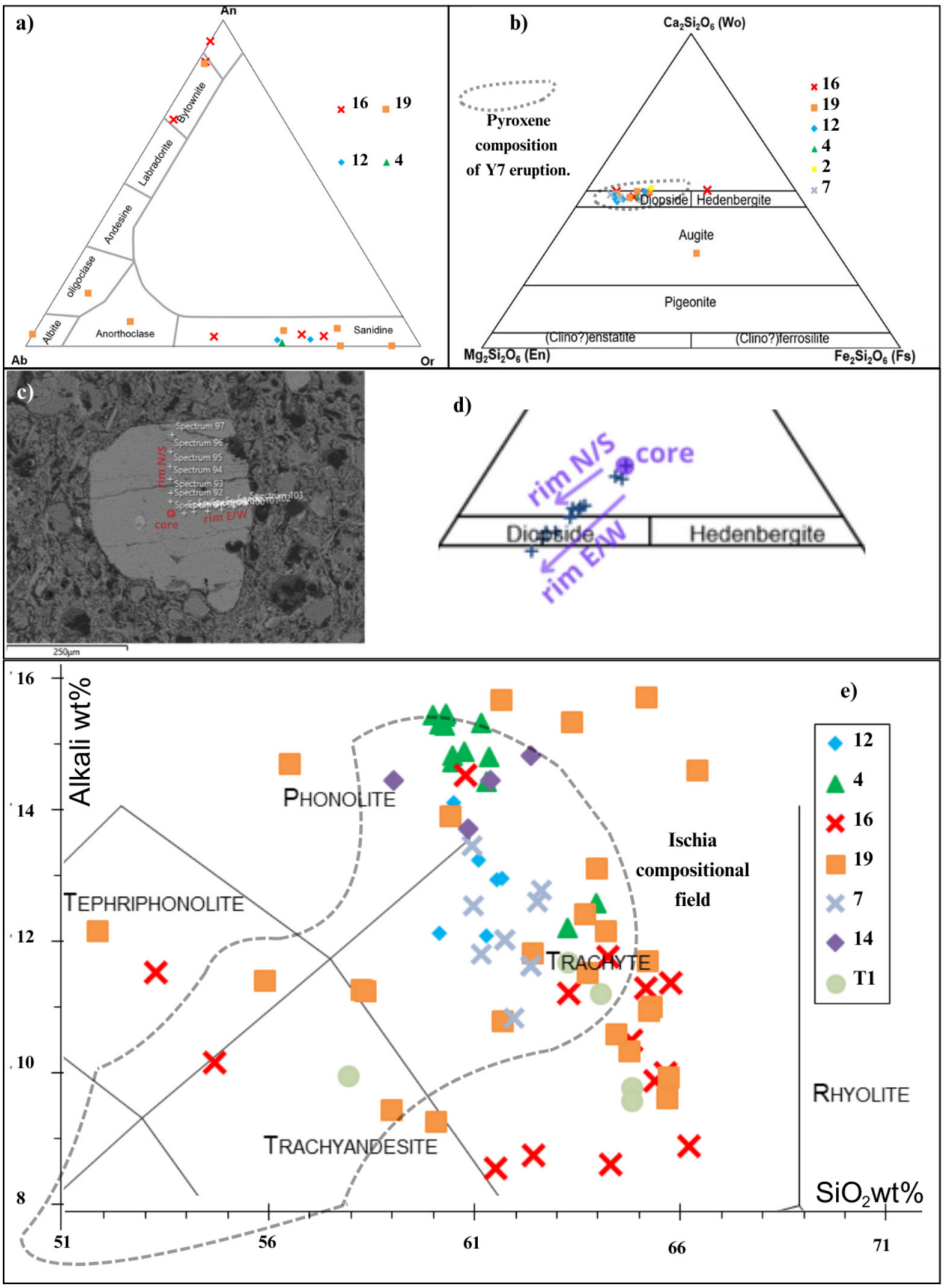

FIGURE 3 | (a) Compositional ternary diagram of anorthite, albite, orthoclase; (b) compositional diagram of phenocrystals of pyroxene with compositional field of pyroxene of Y7 eruption (D'Antonio et al. 2021); (c) point analyses in clinopyroxene of sample 2; (d) compositional data from core to rims; (e) total alkali silica (TAS diagram) with compositional field of Ischia eruptions (R. J. Brown, Civetta, et al. 2014; D'Antonio et al. 2021).

events, volcanic particles of various sizes, mineral compositions and densities are carried by powerful stratospheric winds over long distances before eventually settling and depositing. The deposition behaviour of such particles is primarily determined by their physical properties (size, density, shape) and by environmental factors such as wind advection, gravity and secondary processes such as ash aggregation (Brown et al. 2012) and gravitational instabilities (Manzella et al. 2015). The particle size observed at a specific distance from the volcanic vent depends on several factors, including eruptive energy, column height, wind speed and direction, as well as the distance from the vent. Field studies have enabled the creation of isopleth maps that outline areas with similar maximum particle sizes. Although the Y-7 eruption is one of the most significant eruptions in the Mediterranean area, with an estimated volume of approximately 40 km^3, there are currently no published isopleth maps detailing fallout deposition (D'Antonio et al. 2021; Tomlinson et al. 2014). A rough estimate of how far volcanic materials may have travelled can be determined through a simplified study. In this case, we analyse a specific volcanic particle, such as a bytownite feldspar crystal with a diameter of 0.72 mm and a density of approximately 2600 kg/m^3.

The terminal velocity (v_t) of a feldspar particle with such properties can be calculated using the formula (Scandone and Giacomelli 2004):

$$v_t = \left[\left(8^*\rho_p{}^*r^*g\right)/\left(3^*C_D{}^*\rho_a\right)\right]^{1/2}$$

where ρ_p is the density of the particle, r is the radius of the particle, g is the gravitational acceleration, C_D is the drag coefficient (assumed to be 0.8 for a cubic particle), ρ_a is the air density. The maximum scattering (χ), i.e., the maximum distance that the particle travels relative to the emission center of the eruptive column, can be derived from this simplified relationship (details on used formulae in Supporting Information):

$$\chi = v_w{}^* \left(H/v_t\right)$$

where H is the height of the eruptive column and v_w is the wind speed in m/s in the stratosphere between 20 and 50 km above the Earth's surface. Based on statistics calculated over years of weather data (Bucchignani 2022), these winds can vary between 10–20 and 50 m/s depending on altitude and season (prediction of wind in the lower stratosphere). By varying the height of the column and the wind speed in the stratosphere, the calculated fall distances for the particle with a diameter of 0.72 mm from Ischia are reported in Table 4.

Based on the obtained results, and considering the distances from Ischia to Taranto and Castro, which are 286 and 392 km, respectively, the maximum distance of particle dispersion is likely to be closer to Taranto than to Castro. In fact, to reach Castro, one would need to combine extreme parameters, including maximum eruptive column height and maximum stratospheric wind speed, simultaneously.

To support this hypothesis, the Y-7 eruption with the Minoan eruption of Santorini can be compared, which occurred around 1600 BCE. Both eruptions have the same VEI of 7, but they differ significantly in the volumes of material emitted: approximately 40 km^3 for the Y-7 eruption and between 80 and 100 km^3 for the Minoan eruption.

Research indicates that the volcanic ash from Santorini reached the Black Sea, located 1200 km away, with ash grains having a maximum diameter of 105 μm (Guichard et al. 1993). In contrast, sediment layers from the Minoan eruption found in Lake Gölhisar, which is 400 km from Santorini, show grain sizes of about 150 μm. Larger clasts, similar to the larger particles found in our Castro samples, are quite rare (Eastwood et al. 1999).

Therefore, it is unlikely that the Y-7 eruption from Ischia could have deposited particles as large as 0.7 mm over a distance

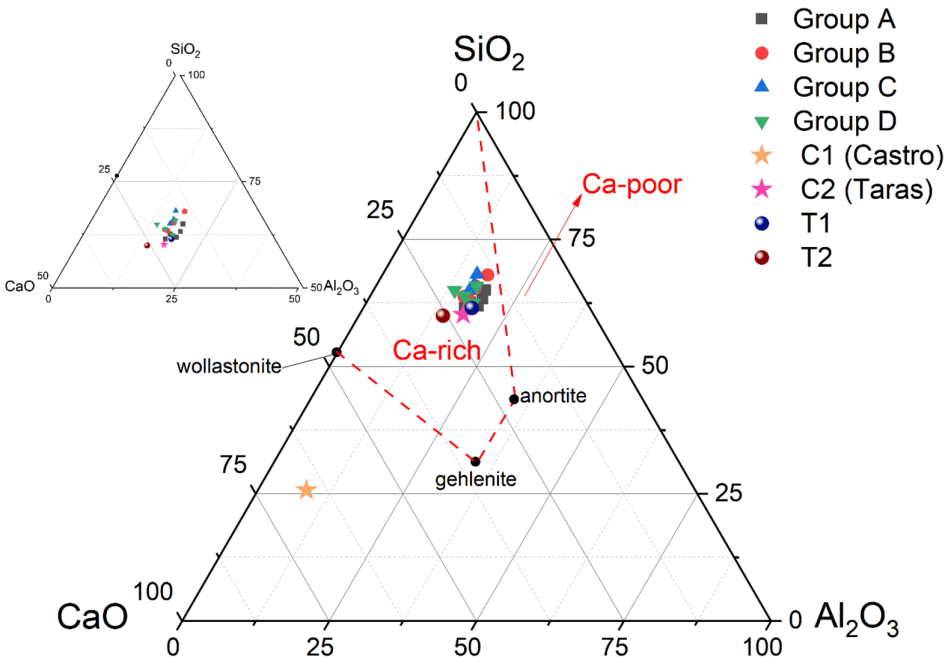

FIGURE 4 | Ternary ACS (Al_2O_3–CaO–SiO_2) diagram showing data of the samples of the four petrographic groups.

TABLE 4 | Results of the dispersion distances for the investigated particle with variable eruption column height and stratospheric wind velocity.

Volcanic column high (km)	Dispersion with vw = 20 m/s (km)	Dispersion with vw = 30 m/s (km)	Dispersion with vw = 40 m/s (km)	Dispersion with vw = 50 m/s (km)
25	140.0	210.1	280.1	350.1
30	168.1	252.1	336.1	420.1
35	196.1	294.1	392.1	490.2
40	224.1	336.1	448.1	560.2

of 400 km. Based on both a simplified calculation of potential fallout areas and comparisons with existing literature on eruptions of similar latitude and magnitude, the Taranto area seems to be a much more plausible source for the collection of raw materials.

5.2 | Equivalent Firing Temperatures

Mineralogical and petrographic studies of ancient terracotta samples have also provided important insights into the firing techniques by observing the optical properties of the clay matrix (Quinn 2013) and the prograde or newly formed mineralogical phases from clayey raw materials with a certain composition (Trindade et al. 2010; El Ouahabi et al. 2015; De Bonis et al. 2013; De Bonis et al. 2014). It is worth noting that, in the mineralogical evaluation of the newly formed minerals, clinopyroxene (diopside) from the volcanic clasts was considered negligible.

Mineralogical analyses indicate that the terracottas of Group D were fired at relatively low temperatures, likely not exceeding 800°C. This conclusion is supported by the high amounts of calcite observed and the presence of identifiable microfossils in the polarized light microscopy (PLM) analyses. Furthermore, the low firing temperature is corroborated by the optical activity observed in these samples. A slightly higher firing temperature (850°C) can be asserted for samples 6 and 7 due to the appearance of pyroxenes and gehlenite, along with prograde phases such as calcite and muscovite/illite.

The terracottas of Group C still show good optical activity and a small amount of calcite (between 7.6% and 10.8%, see Table 2). They were probably fired at higher temperatures than the terracottas of Group D, but not at more than 850°C.

Groups A and B exhibit a significantly lower content of calcite and muscovite when compared to Groups C and D, while displaying an increase in diopside, gehlenite and anorthite. The firing temperatures for Groups A and B are higher than those of the previously mentioned groups, exceeding 850°C–900°C. The optical activity in the mineralogical Groups A and B is very low or absent, which further confirms that their firing temperature was above 850°C. The presence of muscovite/illite suggests that the temperatures for Groups A and B did not exceed 950°C. Based on the amounts of muscovite/illite and calcite, it can be inferred that the terracottas of Group A were subjected to slightly higher temperatures than those of Group B (Table S2).

This hypothesis is also supported by the degrees of sintering observed in the mixtures of the samples in the SEM-EDS analysis. The SEM-EDS analysis confirms the different degrees of sintering of the ceramic body (Figure S4) already observed in the four petrographic groups. Samples 2 and 4, which belong to petrographic Group B, show a low to medium degree of sintering, while samples 12, 16 and 19, which fall into petrographic Group A, show a medium degree of sintering that is slightly higher than that of the samples in petrographic Group B. The samples of Group A have a homogeneous matrix and the structures of the clay minerals, which are recognisable in the samples of Group B, tend to be absent (Gliozzo et al. 2016; Daghmehchi et al. 2023).

Sample 17 has a mineralogical composition similar to Group B but the matrix has an optical activity similar to Group C; the firing temperature is probably between 800°C and 900°C.

6 | Conclusion

The mineralogical, petrographic and chemical analyses of the architectural terracottas from the *Athenaion* at Castro identify four main compositional groups. These differences are most plausibly explained by variations in production technology—particularly firing conditions—rather than by differences in raw material sources. Indeed, all 20 samples are chemically indistinguishable, indicating the use of the same or very similar clay across the assemblage.

Comparative chemical analysis with local clays from Castro and Taranto shows a clear match with the Taranto samples and a marked difference from Castro clays. This suggests that the clay used was sourced from the Taranto area. Further support comes from the presence of volcanic inclusions—linked to the Ischia Y-7 eruption—found in high percentages (20%–50%) in many terracotta samples. The aplastic inclusions are consistent with naturally occurring components of Tarantine clays, since they are attested also in T1 and T2 samples. Recent studies have even suggested the intentional addition of volcanic material sourced from locations at some distance from the production sites to reduce the plasticity of the clay, thereby lowering the risk of cracking and deformation during drying and firing: significant examples are recorded in Gela (Santostefano 2019; Barone et al. 2017), Lentini and Syracuse (Barone et al. 2018; Santostefano 2019). In our case, however, the volcanic material was likely already present in the clay deposits of the Taranto area and was not added intentionally. In conclusion, two production scenarios are therefore plausible: the clay was imported to Castro and used locally to manufacture the terracotta roofs, or the terracotta elements were produced and fired in Taras and then shipped to Castro. This latter hypothesis aligns more closely with the available evidence and finds parallels in documented cases of long-distance transport of architectural terracottas by Greek cities in Southern Italy (Giaccone 2022).

Regarding the production technology, strong correlations between petrographic groupings and archaeological types should be highlighted. **Group A** fully matches the *Classical Roof 2* assemblage (with the exception of sample 13, which falls within Group C, and sample 8, in Group D). **Group B** includes nearly all the materials from *Archaic Roofs 1 and 2* (apart from nos. 14 and 15, which belong to Group C). This consistency appears to suggest similar firing conditions for the two most representative and clearly distinguishable archaeological groups. As for the medium-high firing temperature identified for Groups A and B—ranging between 900°C and 1000°C—the substantial thickness of the pieces (see Table S1) may have necessitated particular care to ensure that the inner portions were adequately fired.

Groups C and D include materials that likely derive from different roofs and cover a broader chronological range. Indeed, Group D contains both Archaic antefixes (9) and Late Classical ones (6); similarly, Group C includes elements from Archaic *simas* (14–15) to Classical antefixes (10). This evidence suggests a certain continuity in the technological know-how over this time span, particularly with regard to the procurement of raw materials and firing techniques. In general, in the *Athenaion* in Castro, there is no evidence of a deliberate strategy aimed at lowering firing temperatures, as observed in the production of architectural terracottas at Capua (Verde et al. 2024). Thus, the lower firing temperature identified for Groups C and D might be linked to the minor size of the terracotta elements, such as the antefixes and crowning elements of *simae*, belonging to simplified roof types, which do not require complex and massive cornice revetments.

In summary, the petrographic and chemical analysis of the architectural terracottas from the *Athenaion* at Castro provides data of considerable significance from multiple perspectives. First, it presents unprecedented evidence of the dispersal of volcanic materials from the Ischia Y-7 eruption in the Taranto area. Secondly, the analysis confirms that artefacts previously attributed to Tarentine workshops on the basis of morphological and stylistic criteria are indeed of Tarentine manufacture. The likely direct importation of fired roofs from the Greek city, ready for on-site assembly, points to a complex operational *chaîne opératoire* and a significant logistical effort. At the same time, this evidence further supports the role of Taras as a significant production centre capable of meeting the demands of the Messapian elites who ruled the *Athenaion*, and influencing the indigenous communities of ancient Salento.

Acknowledgements

The authors would like to thank Prof. Francesco D'Andria (Accademia dei Lincei), director of the Archaeological Museum of Castro and scientific director of the excavations, conducted under the authorization of the Soprintendenza Archeologia, Belle Arti e Paesaggio for the provinces of Brindisi and Lecce (DG ABAP 30.08.2019.914), Laura Chiarantini and Tiziano Catalani for their technical assistance in the SEM-EDS analysis, as well as Pietro Gabellini for helpful discussion on volcanological issues. Open access publishing facilitated by Consiglio Nazionale delle Ricerche, as part of the Wiley - CRUI-CARE agreement.

Funding

Open access publishing facilitated by Consiglio Nazionale delle Ricerche, as part of the Wiley—CRUI-CARE agreement.

Data Availability Statement

The data that supports the findings of this study are available in the supplementary material of this article.

References

Bajnok, K., Z. Kovács, J. Gait, et al. 2022. "Integrated Petrographic and Geochemical Analysis of the Langobard Age Pottery of Szólád, Western Hungary." *Archaeological and Anthropological Sciences* 14: 13. https://doi.org/10.1007/s12520-021-01467-1.

Barone, G., C. M. Belfiore, P. Mazzoleni, A. Pezzino, and M. Viccaro. 2010. "A Volcanic Inclusions Based Approach for Provenance Studies of Archaeological Ceramics: Application to Pottery From Southern Italy." *Journal of Archaeological Science* 37: 713–726. https://doi.org/10.1016/j.jas.2009.11.002.

Barone, G., P. Mazzoleni, S. Raneri, et al. 2018. "Exploring the Coroplasts' 'Techne' in Greek Architectural Terracottas From Sicily: An Archaeometric Approach." *Archaeometry* 60: 986–1001. https://doi.org/10.1111/arcm.12380.

Barone, G., P. Mazzoleni, S. Raneri, G. Spagnolo, and A. Santostefano. 2017. "Coroplastic Art in Sicily: An Investigation on Provenance and Manufacturing Technology of Greek Architectural Terracottas From Gela (Italy)." *Mediterranean Archaeology and Archaeometry* 17, no. 1: 89–101. https://doi.org/10.5281/zenodo.258087.

Berger, E. 1982. *Antike Kunstwerke aus der Sammlung Ludwig II*. Terrakotten und Bronzen Veröffentlichungen des Antikenmuseums Basel 4/2.

Bosellini, A., M. Morsilli, and C. Neri. 1999. "Long-Term Event Stratigraphy of the Apulia Platform Margin (Upper Jurassic to Eocene, Gargano, Southern Italy)." *Journal of Sedimentary Research* 69, no. 16: 1241–1252. https://doi.org/10.1306/d4268b4e-2b26-11d7-8648000102c1865d.

Bossio, A., R. Mazzei, B. Monteforti, and G. Salvatorini. 1997. *Carta Geologica del Salento Sud-Orientale, Scala 1:25.000*. Dip. Scienze della Terra, Univ. Siena.

Brown, R. J., C. Bonadonna, and A. J. Durant. 2012. "A Review of Volcanic Ash Aggregation." *Physics and Chemistry of the Earth* 45: 65–78.

Brown, R. J., L. Civetta, I. Arienzo, et al. 2014. "Geochemical and Isotopic Insights Into the Assembly, Evolution and Disruption of a Magmatic Plumbing System Before and After a Cataclysmic Caldera-Collapse Eruption at Ischia Volcano (Italy)." *Contributions to Mineralogy and Petrology* 168: 1035. https://doi.org/10.1007/s00410-014-1035-1.

Brown, S. K., H. S. Crosweller, R. S. J. Sparks, et al. 2014. "Characterisation of the Quaternary Eruption Record: Analysis of the Large Magnitude Explosive Volcanic Eruptions (LaMEVE) Database." *Journal of Applied Volcanology* 3: 5. https://doi.org/10.1186/2191-5040-3-5.

Bucchignani, E. 2022. "Wind Predictions in the Lower Stratosphere: State of the Art and Application of the COSMO Limited Area Model." *Meteorology* 1: 311–326. https://doi.org/10.3390/meteorology1030020.

Cioni, R., S. Levi, and R. Sulpizio. 2000. "Apulian Bronze Age Pottery as a Long-Distance Indicator of the Avellino Pumice Eruption (Vesuvius, Italy)." *Geological Society, London, Special Publications* 171: 159–177. https://doi.org/10.1144/GSL.SP.2000.171.01.13.

Cristofani, M. 1967. "Le Terrecotte Architettoniche Provenienti dal Santuario di Hera Lacinia a Capocolonna." *Archeologia Classica* 19: 313–319.

Daghmehchi, M., C. Coletti, D. Hyeok Moon, et al. 2023. "Mineralogical and Microstructural Characterization of Ceramics From the Fifth and Fourth Millennium BC in the Central Plateau of Iran." *Open Ceramics* 15: 100427. https://doi.org/10.1016/j.oceram.2023.100427.

D'Andria, F. 2009. *Castrum Minervae (Archeologia e Storia 9)*. Congedo Editore.

D'Andria, F. 2020. "L'Athenaion di Castro in Messapia." *Mitteilungen des Deutschen Archäologischen Instituts. Römische Abteilung* 126: 79–140.

D'Andria, F., E. Degl'Innocenti, M. P. Caggia, T. Ismaelli, and L. Mancini. 2023. *Athenaion: Tarantini, Messapi e Altri nel Santuario di Atena a Castro. Catalogo Della Mostra*. Edipuglia.

D'Antonio, M., I. Arienzo, R. J. Brown, P. Petrosino, C. Pelullo, and B. Giaccio. 2021. "Petrography and Mineral Chemistry of Monte Epomeo Green Tuff, Ischia Island, South Italy: Constraints for Identification of the Y-7 Tephrostratigraphic Marker in Distal Sequences of the Central Mediterranean." *Minerals* 11: 955. https://doi.org/10.3390/min11090955.

De Bonis, A., G. Cultrone, C. Grifa, A. Langella, and V. Morra. 2014. "Clays From the Bay of Naples (Italy): New Insight on Ancient and Traditional Ceramics." *Journal of the European Ceramic Society* 34: 3229–3244. https://doi.org/10.1016/j.jeurceramsoc.2014.04.014.

De Bonis, A., C. Grifa, G. Cultrone, P. De Vita, A. Langella, and V. Morra. 2013. "Raw Materials for Archaeological Pottery From the Campania Region of Italy: A Petrophysical Characterization." *Geoarchaeology* 28: 478–503. https://doi.org/10.1002/gea.21450.

De Marco, A., M. Moresi, and G. Nuovo. 1981. "Le Argille dei Bacini di Taranto e di Grottaglie-Montemesola: Caratteri Granulometrici, Mineralogici e Chimici." *Società Italiana di Mineralogia e Petrologia* 37, no. 1: 241–266.

De Santis, V., and M. Caldara. 2015. "The 5.5–4.5 kyr Climatic Transition as Recorded by the Sedimentation Pattern of Coastal Deposits of the Apulia Region, Southern Italy." *Holocene* 25: 1313–1329. https://doi.org/10.1177/0959683615584207.

Deer, W. A., R. A. Howie, and J. Zussman. 2013. *An Introduction to the Rock-Forming Minerals*. Third ed. Minerological Society.

Dell'Aglio, A., and A. Zingariello. 2015. *MARTA. Il Museo Nazionale Archeologico di Taranto*. Scorpione Ed.

Donato, P., R. De Rosa, M. Tenuta, R. S. Iovine, F. Totaro, and M. D'Antonio. 2022. "Sr-Nd Isotopic Composition of Pyroxenes as a Provenance Indicator of a Double-Volcanic Source in Sands of the Ofanto River (Southern Italy)." *Minerals* 12: 232. https://doi.org/10.3390/min12020232.

Eastwood, W. J., N. J. G. Pearce, J. A. Westgate, W. T. Perkins, H. F. Lamb, and N. Roberts. 1999. "Geochemistry of Santorini Tephra in Lake Sediments From Southwest Turkey." *Global and Planetary Change* 21: 17–29. https://doi.org/10.1016/S0921-8181(99)00005-3.

El Ouahabi, M., L. Daoudi, F. Hatert, and N. Fagel. 2015. "Modified Mineral Phases During Clay Ceramic Firing." *Clays and Clay Minerals* 63: 404–413. https://doi.org/10.1346/CCMN.2015.0630506.

Germinario, C., G. Cultrone, L. Cavassa, et al. 2019. "Local Production and Imitations of Late Roman Pottery From a Well in the Roman Necropolis of Cuma in Naples, Italy." *Geoarchaeology* 34: 62–79. https://doi.org/10.1002/gea.21703.

Giaccone, N. 2022. "L'esportazione di Terrecotte Architettoniche su Lunghe Distanze nel Mondo Greco." *Agoghé/Αγωγή* 19: 43–49.

Gliozzo, E., G. Baldassarre, M. Turchiano, and I. Turbanti Memmi. 2016. "From the Kilns to the Fair: Producing Building Materials at Faragola and Canusium (Northern Apulia, Italy)." *Archaeological and Anthropological Sciences* 8: 705–729. https://doi.org/10.1007/s12520-015-0249-0.

Guichard, F., S. Carey, M. A. Arthur, H. Sigurdsson, and M. Arnold. 1993. "Tephra From the Minoan Eruption of Santorini in Sediments of the Black Sea." *Nature* 363: 610–612. https://doi.org/10.1038/363610a0.

Ismaelli, T. 2023. "Riflessi dell'Architettura Tarantina a Castro." In: D'andria et al. 2023, 125–131.

Izzo, F., V. Guarino, A. Ciotola, et al. 2021. "An Archaeometric Investigation in a Consumption Context: Exotic, Imitation and Traditional Ceramic Productions From the Forum of Cumae (Southern Italy)." *Journal of Archaeological Science: Reports* 35: 102768. https://doi.org/10.1016/j.jasrep.2020.102768.

Laviosa, C. 1954. "Le Antefisse Fittili di Taranto." *Archeologia Classica* 6: 217–250.

Le Bas, M. J., R. W. Le Maitre, A. Streckeisen, and B. Zanettin. 1986. "A Chemical Classification of Volcanic Rock Based on the Total Alkali-Silica Diagram." *Journal of Petrology* 27: 745–750.

Levin, E. M., C. R. Robbins, and H. F. McMurdie. 1964. *Phase Diagrams for Ceramists*. American Ceramic Society, Inc.

Lisco, S., C. Corselli, F. De Giosa, et al. 2016. "Geology of Mar Piccolo, Taranto (Southern Italy): The Physical Basis for Remediation of a Polluted Marine Area." *Journal of Maps* 12: 173–180. https://doi.org/10.1080/17445647.2014.999136.

Magrini, D., E. Cantisani, S. Vettori, F. Buti, C. Conti, and E. Possenti. 2023. "Il Colore di Atena: Policromia su Materiali Lapidei e Terrecotte." In: D'andria et al. 2023 183–187.

Manzella, I., C. Bonadonna, J. C. Phillips, and H. Monnard. 2015. "The Role of Gravitational Instabilities in Deposition of Volcanic Ash." *Geology* 43, no. 3: 211–214.

Melluso, L., V. Morra, V. Guarino, R. De' Gennaro, L. Franciosi, and C. Grifa. 2014. "The Crystallization of Shoshonitic to Peralkaline Trachyphonolitic Magmas in a H_2O–Cl–F-Rich Environment at Ischia (Italy), With Implications for the Feeder System of the Campania Plain Volcanoes." *Lithos* 210: 242–259. https://doi.org/10.1016/j.lithos.2014.10.002.

Mertens-Horn, M. 1988. *Die Löwenkopf-Wasserspeier des Griechischen Westens im 6. und 5. Jahrhundert v. Chr. im Vergleich mit den Löwen des Griechischen Mutterlandes*, Mitteilungen des Deutschen Archäologischen Instituts, Römische Abteilung. Ergänzungsheft 28.

Morimoto, N., J. Fabries, A. K. Ferguson, et al. 1988. "Nomenclature of Pyroxenes." *American Mineralogist* 73: 1123–1133.

Ohbuchi, A., K. Otori, K. Hagiwara, Y. Koike, and T. Nakamura. 2021. "Phase Quantification of Regular and Turbo-Stratified Graphite in Cast Iron by X-Ray Diffractometry/Rietveld Refinement." *ISIJ International* 61: 2249–2255. https://doi.org/10.2355/isijinternational.ISIJINT-2021-070.

Pérez-Monserrat, E. M., L. Maritan, V. Baratella, and M. Vidale. 2023. "Production Technologies and Provenance of Ceramic Materials From the Earliest Foundry of Pre-Roman Padua, NE Italy." *Heritage* 6: 2956–2977. https://doi.org/10.3390/heritage6030157.

Pouchou, J. L., and F. Pichoir. 1991. "Quantitative Analysis of Homogeneous or Stratified Microvolumes Applying the Model "PAP"." In *Electron Probe Quantification*, edited by K. F. J. Heinrich and D. E. Newbury, 31–75. Plenum Press. https://doi.org/10.1007/978-1-4899-2617-3_4.

Quinn, P. S. 2009. *Interpreting Silent Artefacts: Petrographic Approaches to Archaeological Ceramics*. Archaeopress.

Quinn, P. S. 2013. *Ceramic Petrography: The Interpretation of Archaeological Pottery and Related Artefacts in Thin-Sections*. Archaeopress.

Rescigno, C. 2023. "Le Terrecotte Architettoniche di Provenienza Tarantina del MArTA: Modelli, Sistemi Decorativi, Soluzioni Artigianali." In: D'andria et al. 2023, 133–137.

Rodríguez, C., R. Bermúdez Coronel-Prats, G. Barone, G. Cultrone, P. Mazzoleni, and D. Tanasi. 2015. "Petrographic and Chemical Characterization of Bronze Age Pottery From the Settlement of Mount san Paolillo (Catania, Italy)." *Rendiconti Lincei* 26: 485–497.

Sansò, P., S. Margiotta, G. Mastronuzzi, and A. Vitale. 2015. "The Geological Heritage of Salento Leccese Area (Apulia, Southern Italy)." *Geoheritage* 7: 85–101. https://doi.org/10.1007/s12371-013-0093-5.

Santostefano, A. 2019. "Tra Sapere Tecnico e Sperimentazione: la Fabbrica di Gela attraverso l'analisi di Terrecotte Architettoniche da due Aree Santuariali." In *Deliciae Fictiles. V, Networks and Workshops: Architectural Terracottas and Decorative Roof Systems in Italy and Beyond*, 165–177. Oxbow Books.

Scandone, R. and L. Giacomelli. 2004. "Vulcanologia. Principi Fisici e Metodi d'Indagine." Collana: Basic. ed. ISBN: 9788820726874.

Tomlinson, E. L., P. G. Albert, S. Wulf, et al. 2014. "Age and Geochemistry of Tephra Layers From Ischia, Italy: Constraints From Proximal-Distal Correlations With Lago Grande di Monticchio." *Journal of Volcanology and Geothermal Research* 287: 22–39. https://doi.org/10.1016/j.jvolgeores.2014.09.006.

Trindade, M. J., M. I. Dias, J. Coroado, and F. Rocha. 2010. "Firing Tests on Clay-Rich Raw Materials From the Algarve Basin (Southern Portugal): Study of Mineral Transformations With Temperature." *Clays and Clay Minerals* 58: 188–204. https://doi.org/10.1346/CCMN.2010.0580205.

Valenzano, E., G. Scardino, G. Cipriano, et al. 2018. "Holocene Morpho-Sedimentary Evolution of the Mar Piccolo Basin (Taranto, Southern Italy)." *Geografia Fisica e Dinamica Quaternaria* 41: 119–135. https://doi.org/10.4461/GFDQ.2018.41.8.

Verde, M., A. De Bonis, N. Wagner, F. d'Aniello, and V. Morra. 2024. "Decoding Capua's Roof Terracotta: A Multi-Analytical Study of the Fondo Patturelli Sanctuary and Alveo Marotta Furnace (6th Century BCE – 1st Century BCE)." *Journal of Archaeological Science: Reports* 58: 104708. https://doi.org/10.1016/j.jasrep.2024.104708.

Vineberg, S. O., R. Isaia, P. G. Albert, R. J. Brown, and V. C. Smith. 2023. "Insights Into the Explosive Eruption History of the Campanian Volcanoes Prior to the Campanian Ignimbrite Eruption." *Journal of Volcanology and Geothermal Research* 443: 107915. https://doi.org/10.1016/j.jvolgeores.2023.107915.

Whitbread, I. K. 1989. "A Proposal for the Systematic Description of Thin Sections Towards the Study of Ancient Ceramic Technology." In *Proceedings of the 25th International Symposium of Archaeometry*, edited by Y. Maniatis, 127–138. Elsevier.

Whitney, D. L., and B. W. Evans. 2010. "Abbreviations for Names of Rock-Forming Minerals." *American Mineralogist* 95: 185–187. https://doi.org/10.2138/am.2010.3371.

Supporting Information

Additional supporting information can be found online in the Supporting Information section. **Figure S1:** Rietveld refinement of samples representative of each Group sample 16 Group A, sample 4 Group B, sample 10 Group C, sample 6 Group D. **Figure S2:** Stacked columns graphs of a) major and b) minor and trace elements of the terracotta samples. Major elements are normalized to 100%. **Figure S3:** Dispersal area of the Y-7 eruption (Ischia island). **Figure S4:** Sintering degree of a) Group B, sample 4 that is lower than b) Group A, sample 12. **Table S1:** Microchemical data (wt%) obtained from SEM EDS analyses. **Table S2:** Firing temperatures obtained by mineralogical composition and optical activity of each terracotta sample. The temperature data are followed by the thickness of the samples and the archaeological dating. **Data S1:** Supporting information.